Materials for Renewable and Sustainable Energy (2025) 14:54
https://doi.org/10.1007/s40243-025-00330-w

REVIEW PAPER

Modified high hardness steel coating for biomass corrosion protection

Alina Agüero[1] · Marcos Gutiérrez[1] · Pauline Audigié[1] · Sergio Rodríguez[1] · Jon Pascual[1]

Received: 16 May 2025 / Accepted: 21 August 2025 / Published online: 13 September 2025
© The Author(s) 2025

Abstract
Biomass is a renewable and CO_2-neutral energy source. However, the efficiency of biomass combustion plants remains lower than that of current fossil fuel-based systems. To minimize corrosion from aggressive species found in biomass combustion, these plants currently operate at a maximum temperature of 550 °C. The European project BELENUS explored new materials and coatings to raise the operating temperature to 600 °C, thereby improving plant efficiency. Among the coatings under investigation, a super high-hardness steel (SHS) modified with Al, applied by high velocity oxy-fuel (HVOF) thermal spray on ferritic steel SVM12, has demonstrated an improved performance in the laboratory, exposed to a model biomass environment containing KCl deposits for 8000 h at 600 °C. Microstructural analysis by field emission scanning electron microscopy (FESEM) and X-ray diffraction was conducted on the tested samples to examine the coating's evolution in these environments, as well as the associated protection and degradation mechanisms. The presence of Al within the coating significantly enhanced its resistance to biomass corrosion when compared to uncoated SVM12 and the Al-free SHS coating. Possible reasons for the improved behaviour of the Al-modified coating are the reduction of porosity as well as the blocking effect of either intermetallic FeAl or Al oxide which forms at the splat boundaries prior to exposure to the corrosive atmosphere.

Keywords Biomass corrosion · HVOF thermal spray · Coatings · Steel · Alumina

Introduction

Biomass is one of the currently available renewable energy sources and presents several advantages, including widespread availability and lower costs compared to fossil fuels. It can be used to produce biofuels for heating or transportation [1, 2] or simply directly as a fuel to be burnt for producing electricity and heat [3]. As a result, it contributes to reducing dependence on fossil fuels. Additionally, coal-fired power plants can be readily adapted for biomass combustion. Biomass is considered carbon neutral, as it recaptures the CO_2 released during combustion, and it also adds value to waste by reducing landfill accumulation. However, one of the major challenges associated with biomass combustion is its high corrosivity, and in particular, its impact on superheater tubes. To mitigate corrosion, current power plants are limited to a maximum operating temperature of 550 °C, which consequently lowers the overall plant efficiency. Furthermore, the durability of boiler components in biomass-fired plants is generally reduced compared to those in coal-fired systems. Therefore, the use of highly corrosion-resistant materials and advanced coating technologies is essential to enhance both the longevity and performance of biomass power plants.

Corrosion resulting from biomass combustion is a complex issue, as boilers may burn a wide variety of biomass or waste fuels, including municipal solid waste and agricultural or forestry residues such as straw, peat, wood chips, bark, and rice husks. This variability in fuel types significantly influences the operating conditions of the plant. In the European Union, biomass feedstocks are generally categorized into three main groups based on their source: (i) agriculture, (ii) forestry, and (iii) waste, with further classifications according to biomass categories and types, each with general and specific definitions [4].

Moreover, the chemical composition of biomass varies depending on the specific plant species and its geographical origin (country or region). Compounds such as potassium

✉ Alina Agüero
agueroba@inta.es

[1] Department of Materials and Structures, Instituto Nacional de Técnica Aeroespacial (INTA), 28850 Torrejón de Ardoz, Madrid, Spain

chloride (KCl), hydrogen chloride (HCl), and sulfur dioxide (SO_2), which are released during biomass combustion, are among the most corrosive species [5]. The presence of alkali and alkaline earth metals in biomass is also known to contribute significantly to corrosion processes [6].

To enhance boiler efficiency and improve the durability of boiler components, careful material selection is essential to prevent or mitigate high-temperature corrosion, particularly in superheater and water-wall tubes. Austenitic stainless steels such as 310S and high-performance alloys like Alloy 625 have been increasingly employed for superheater applications due to their superior corrosion resistance. However, these materials are significantly more expensive—ranging from approximately 3–40 times the cost of ferritic steels such as T92. Although T92 can mechanically withstand temperatures up to 600 °C, it exhibits very poor corrosion resistance under biomass combustion conditions [7].

The use of protective coatings can further enhance corrosion resistance relative to the underlying substrate materials, and may substantially reduce both capital (CAPEX) and operational (OPEX) expenditures. For example, the cost of a 3-m tube with a welded overlay of Alloy 625 on a T91 substrate is approximately ten times lower than that of a 3-m tube made entirely of bulk Alloy 625 [7]. Furthermore, by simply reducing the frequency of plant shutdowns, OPEX can be significantly decreased.

Coatings such as Ni-based alloy 625 applied via overlay welding or laser cladding, as well as thermal spray coatings, are currently employed for corrosion protection in biomass boilers [8]. However, both coating technologies can lead to component distortion and surface geometry irregularities. Additionally, under typical boiler operating conditions, these coatings may undergo active oxidation at appreciable rates [9]. In the case of thermal spray coatings, splat boundary porosity, which is inherent to this coating application technology, can create pathways for corrosive species to penetrate and reach the substrate, potentially compromising its integrity.

HVOF coatings have been investigated for protection against steam oxidation [10], coal combustion corrosion [11] and co-firing environments involving biomass [12–14], among other harsh operating conditions. These studies have consistently demonstrated that HVOF coatings offer superior corrosion resistance compared to the underlying ferritic steels. Under biomass combustion, some degree of coating attack invariably occurs, regardless of the coating composition, likely attributable to the inherent porosity present in the microstructure of these coatings, as above mentioned. For instance, Ni20Cr, Fe50Cr and Ni5Al coatings applied by HVOF thermal spraying were exposed to a biomass oxy-combustion model atmosphere at 550 °C for up to 528 h [13]. Both Ni20Cr and Fe50Cr coatings exhibited excellent corrosion resistance, whereas Ni5Al rapidly corroded. The best behaviour was observed for the Fe50Cr coatings, in which no coating penetration was observed. This behaviour was attributed to the presence of $(Cr, Fe)_3O_4$ located at the splat boundaries throughout the coating, as a result of "in-flight" oxidation during the coating deposition process. The presence of these oxides may act as effective barrier to splat boundary corrosion.

Bai et al. [15] applied NiAl coatings by HVOF onto SS304, and exposed them to a synthetic gas containing 500 ppm HCl with a 10 wt% KCl ash deposit at 700 °C for 250 h. Corrosion was observed at the coating/steel interface, which the authors attributed to the diffusion of corrosive species through the coating. They concluded that it is essential to avoid any direct exposure of the coating/substrate interface to Cl_2/O_2 gas. Other HVOF deposited coatings such as CoNiCrAlY, NiMoCrW and NiCr, were also tested in contact with a NaCl-KCl salt mixture at 650 °C for 360 h [16]. Again, these coatings behaved better that the uncoated substrates (T24 and T92) although they all developed corrosive products and exhibited varying degrees of coating penetration. Among them, NiMoCrW showed the best performance, while NiCr showed the poorest. In a separate study, high velocity air fuelled (HVAF) thermal sprayed NiAl, NiCr and NiCrAlY coatings were evaluated by Eklund and coworkers, exposing them to a model atmosphere under KCl deposits for 168 h at 600 °C [17]. NiAl and NiCrAlY exhibited the best behaviour, in particular NiAl which prevented O and Cl through-thickness diffusion. It is noteworthy that all these favorable results were obtained after relatively short exposure durations, which are significantly shorter than the expected service lifetimes of coatings in operational power plant environments.

During the European project "Lowering Costs by Improving Efficiencies in Biomass Fuelled Boilers: New Materials and Coatings to Reduce Corrosion—BELENUS"[18], a range of coatings produced by different deposition technologies were developed and evaluated under various testing conditions: a) at the laboratory, under a model atmosphere with KCl deposits, b) in pilot plants burning three different types of biomass and c) in an operating plant burning various biomass types. Among the coatings tested, a modified super high hardness steel (SHS) exhibited the best results [18]. This coating was deposited by HVOF thermal spray using a commercial powder to which Al powder was added. As a result, metallic Al filled splat boundaries were present within this coating, and when heated prior to testing, Al either oxidized forming alumina or became a Fe aluminide by reaction with the steel splats. In this manner, the splat boundary porosity can be significantly reduced. This paper presents a detailed characterization of the as-deposited Al-modified coating as well as its evolution during testing under a biomass model atmosphere at 600 °C for up to 8000 h, comparing it with the coating produced without Al addition.

Table 1 Nominal composition of SVM12 steel (wt%)

	Fe	C	Mn	Si	Cr	Mo	V	Ni	B	N	Co	W	Nb
Min	Bal	0.10	0.30	0.20	10.50	0.10	0.15	Max	0.008	0.002	1.50	1.50	0.02
Max	Bal	0.16	0.80	0.60	12.00	0.60	0.30	0.40	0.015	0.020	2.50	2.50	0.10

Material and methods

Materials and coating deposition

The base material used in this work is a martensitic/ferritic steel supplied by Vallourec in the form of a tube section, designated as (X13CrCoWMoVNbBN11-2-2; SEL.-No.: 1.4965). The composition of the steel is provided in Table 1. Samples were cut and machined from the tube wall obtaining a final geometry of 20 × 10 × 3 mm coupons.

The metallic coatings tested in this work were deposited using a Sulzer Metco Diamond Jet Hybrid HVOF unit, mounted on a six-axis IRB2400 robot (ABB) and fed by a dual-rotation powder feeder. The torch is equipped with a water-cooling system. The flame is generated by the combustion of H_2(g), while N_2(g) is supplied as a shielding gas to prevent oxidation of the sprayed powder. The powder feed is also carried out with N_2(g). The deposition parameters are summarized in Table 2.

The powder used to produce the SHS coating was WEARTECH SHS 8000HV, supplied by LINCOLN ELECTRIC. Its composition is shown on Table 3. Al-104 powder, supplied by PRAXAIR, was also used to produce the Al-modified SHS coating. Both powders were thoroughly mixed prior to spraying. Before coating, the samples were sand-blasted with corundum and mounted on a holder placed onto a rotating table.

Characterization

The phase analysis of the coatings was determined using X-ray diffraction (XRD) in a PANalytical X'Pert PRO MRD diffractometer, using the Powder Diffraction and Standards (JCPDS) databases for reference.

Cross-sectional microstructural observations were obtained by cutting the specimens with a diamond wheel (ATM 92002401), embedding them in conductive resin (Konductomet, Buehler) and polishing with colloidal silica (MarterPolish2, Buehler). Cross-sections of both as-deposited and oxidized coatings were observed by field emission scanning electron microscopy (FESEM) employing a ThermoScientific APREO C-LV microscope, equipped with an energy-dispersive X-ray microanalysis system (EDX) from Aztec Oxford. Thicknesses were measured by averaging a minimum of 20 measurements taking along the sample.

Table 2 HVOF spray parameters

Oxygen flow (l/min)	Hydrogen flow (l/min)	Powder feed rate (g/min)	Stand-off distance (mm)	Sample rotation speed (mm/s)
200	717	25	150	270

Table 3 Chemical composition (wt%) of the SHS commercial power (WEARTECH SHS 8000HV)

Fe	C	Cr	B	Mo	Mn	Si
Bal.	<4	<25	<5	<6	<3	<2

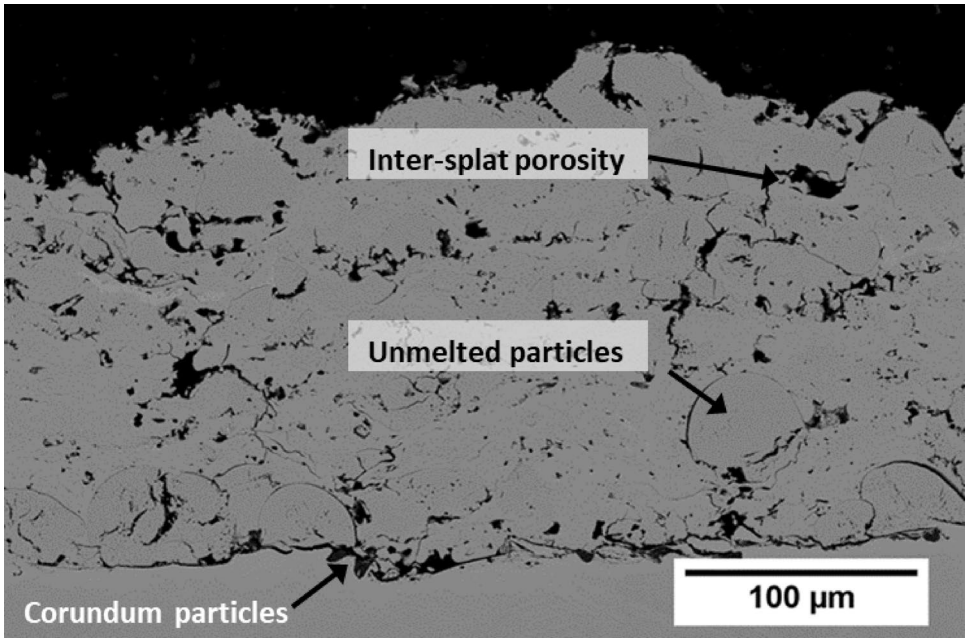


Fig. 1 FESEM cross-section of the SHS coating applied by HVOF thermal spray on SVM12

Laboratory testing

The laboratory biomass corrosion test was designed based on results obtained from a preliminary study and round-robin tests conducted in collaboration with partners from the European project BELENUS. To minimize KCl volatilization from the samples, a crucible containing 3 g of KCl was placed immediately upstream, maintained at the same temperature as the samples. The tests were performed isothermally using INTA's self-designed rig, and the samples were cooled down to room temperature before weighing. Three specimens per coating and condition were tested to ensure reproducibility. Further details on the exposure setup can be found elsewhere [19].

Results

Initial coating characterization

The coating produced with the commercial powder is based on an iron-based nanocomposite containing an amorphous phase, and it exhibits a nanoscale microstructure after spraying. It is mostly used as a wear-resistant coating, offering enhanced hardness and corrosion resistance compared to, for instance, hard Cr coatings [20]. The microstructure of the as-deposited pure SHS coating, with a thickness of ≈200 µm, is shown in Fig. 1. It exhibits typical defects that characterizes thermally spray coatings, such as unmelted particles and inter-splat porosity. The level of porosity was ≅ 8% (calculated by ImageJ software). Corundum particles, used to prepare the substrate surface prior to coating, are also observed embedded within the substrate. The corresponding XRD pattern (not shown) presents broad, low-intensity peaks, evidencing the amorphous/nanocrystalline nature of the coating and these peaks are attributed to the α-FeCr phase.

The 8 wt % Al modified SHS coating was sprayed using the corresponding powder mixture. The resulting coating, approximately 450 µm thick, still exhibits defects such as unmelted particles and corundum particles embedded in the substrate, but a significant reduction of porosity is observed (< 1% according to ImageJ) as Al is distributed along the splat boundaries closing pores (Fig. 2). It appears that during spraying, molten Al may have wetted the surface of the semi-molten SHS powder particles. Notably, this coating is considerably thicker than the one without Al, as it was produced using the same coating parameters but with a higher number of spraying passes. The microscopic investigation reveals that Al remains mostly unreacted, as evidenced by the element mapping and the XRD pattern (Fig. 3), despite the high temperatures reached during the in-flight thermal spraying process. Indeed, Al was detected (98 wt %) within the splats boundary regions, whereas the composition within the coating splats, measured by EDS, was 70 wt % Fe, 20

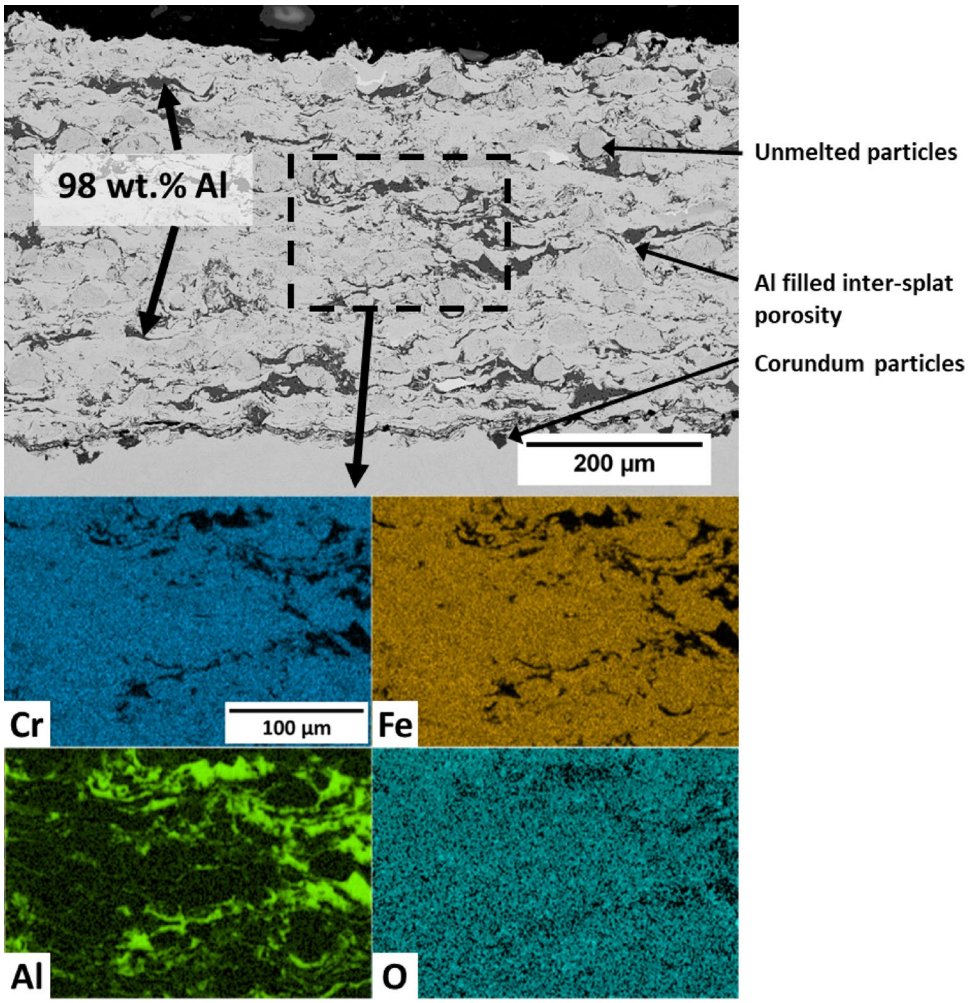


Fig. 2 FESEM cross-section image and element mapping of the as-deposited Al-modified SHS coating applied by HVOF thermal spray on SVM12

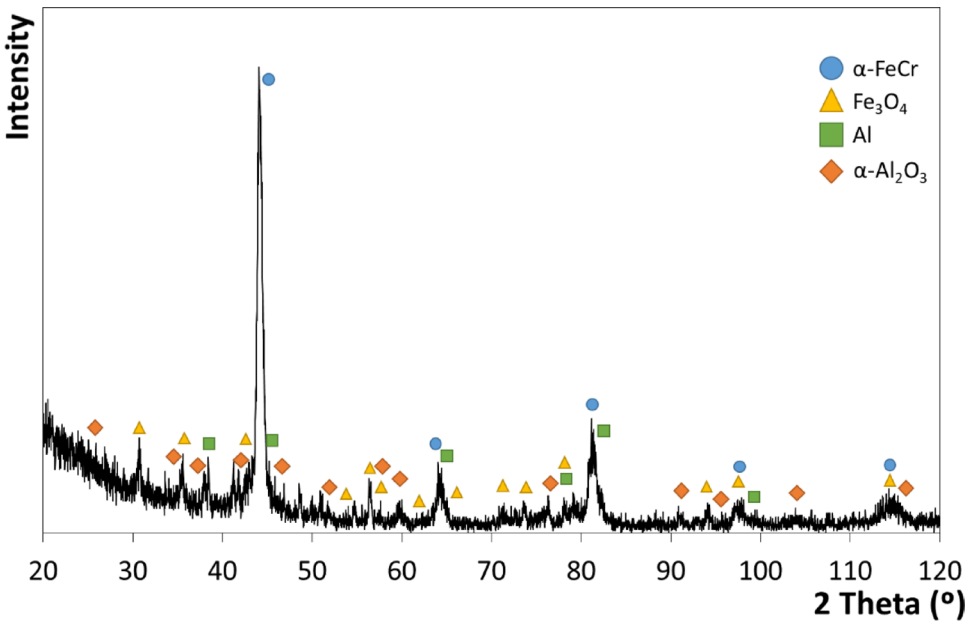


Fig. 3 XRD pattern of the as-deposited Al-modified SHS coating applied by HVOF thermal spray on SVM12

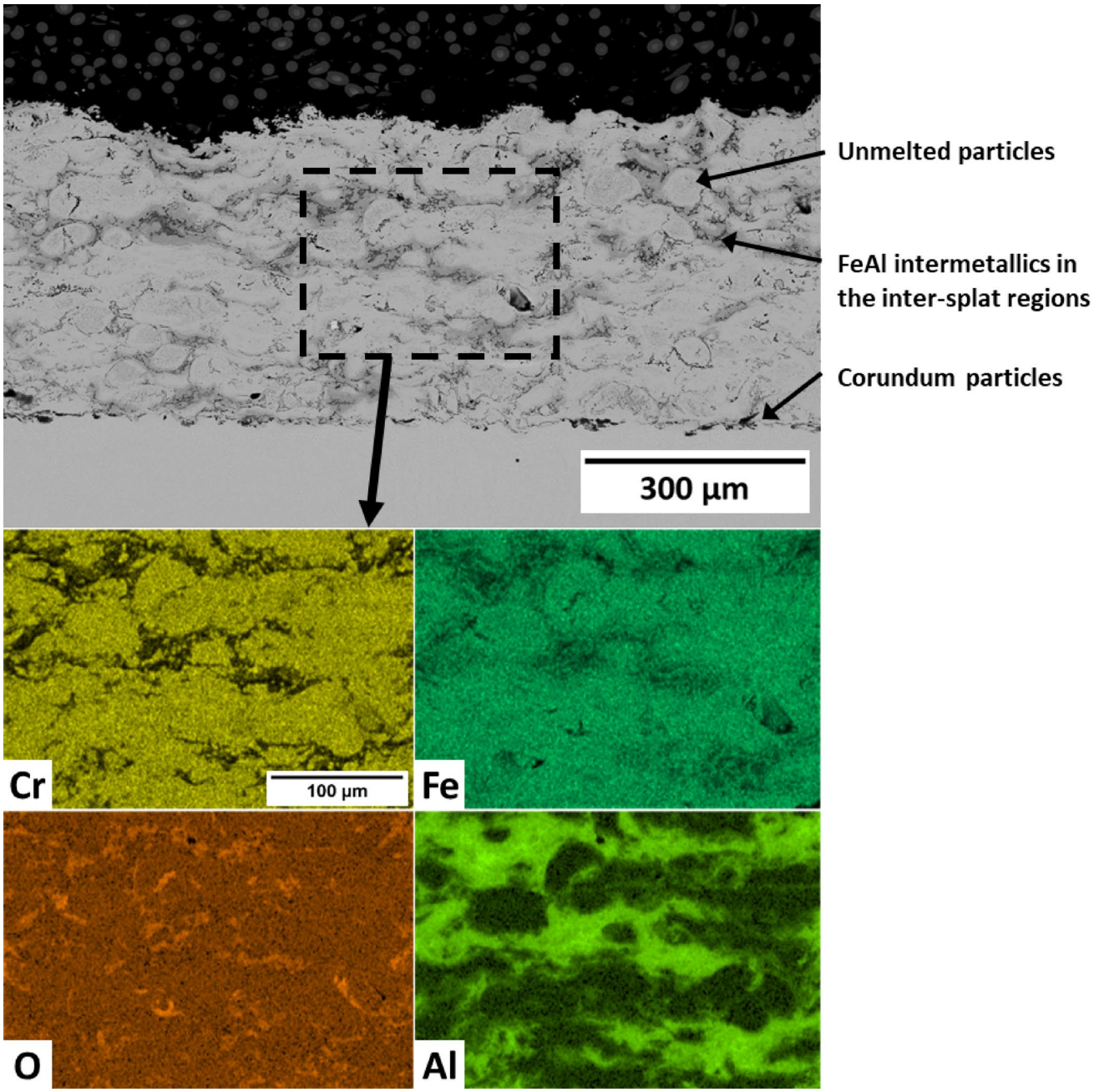


Fig. 4 FESEM cross-section image and element mapping of the Al-modified SHS coating applied by HVOF thermal spray on SVM12 after heat treatment for 10 h at 700 °C under argon atmosphere

wt% Cr, 10 wt% (Mo,Nb), consistent with the corresponding powder nominal composition. Some in-flight internal oxidation may have occurred during the thermal spray process. The XRD diffraction pattern shows low-intensity peaks that can be attributed to α-Al_2O_3 and Fe_3O_4, alongside higher intensity peaks assigned to the α-FeCr phase, with less intense peaks associated to metallic Al (Fig. 3).

Prior to testing, the Al-modified SHS coating was heat-treated for 10 h at 700 °C under argon atmosphere. As a result, Al interdiffused with the coating's steel splats, leading to the formation of Al–Fe intermetallics (Fig. 4). The coating still shows a thickness of approximately 450 µm, and it can be observed that Al has penetrated the coating splats through interdiffusion (Fig. 5). Point analysis at these

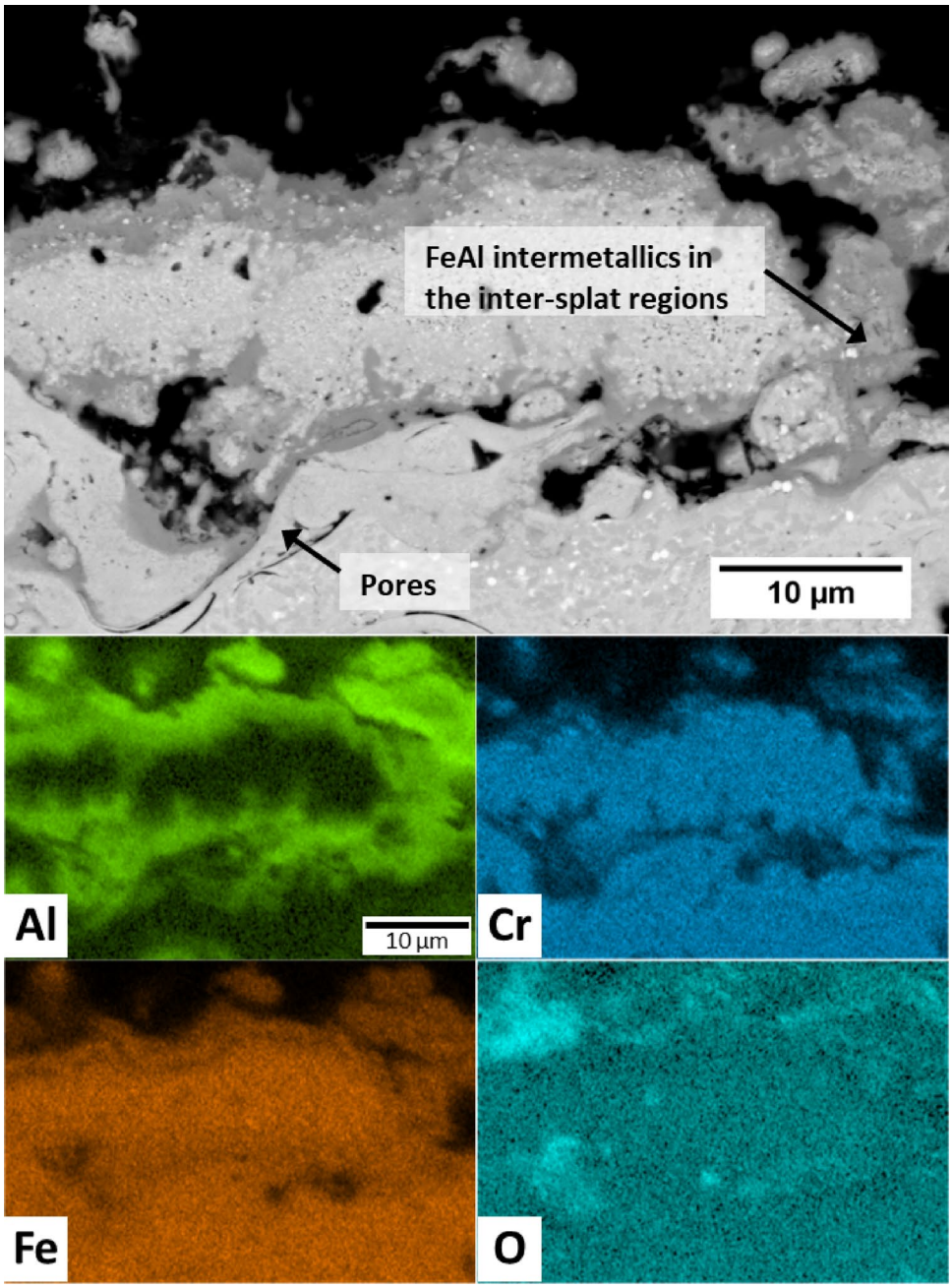


Fig. 5 Surface zone of the Al-modified SHS coating applied by HVOF thermal spray on SVM12 after heat treatment for 10 h at 700 °C under argon atmosphere

areas reveals varying Fe, Al and Cr contents depending on position. The XRD pattern includes peaks attributed to FeAl as well as α-Al_2O_3 (relatively high) and Fe_2O_3, in addition to the α-FeCr coating peaks (Fig. 6). During the heat treatment under Ar, residual oxygen present in the atmosphere reacted with Al present within the coating, resulting in the formation of α-Al_2O_3 as indicated by the element mapping shown in Fig. 5. This oxide is located within splats boundaries and also appears to cover the coating surface.

Test results under a biomass corrosion model atmosphere in the laboratory

Uncoated SVM12

After exposure at 600 °C, uncoated SVM12 suffered significant corrosion, as illustrated on Fig. 7a, where the cross-sectional FESEM image of a sample exposed for 1000 h is shown. A very thick multi-layered oxide scale has been

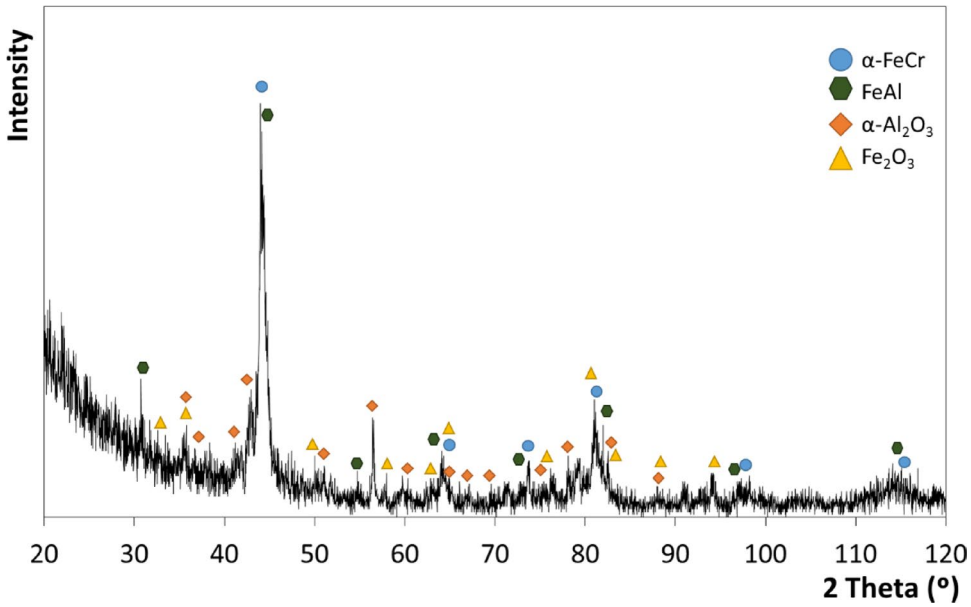


Fig. 6 XRD pattern of the as-deposited Al-modified SHS coating applied by HVOF thermal spray on SVM12 after heat treatment for 10 h at 700 °C under argon atmosphere

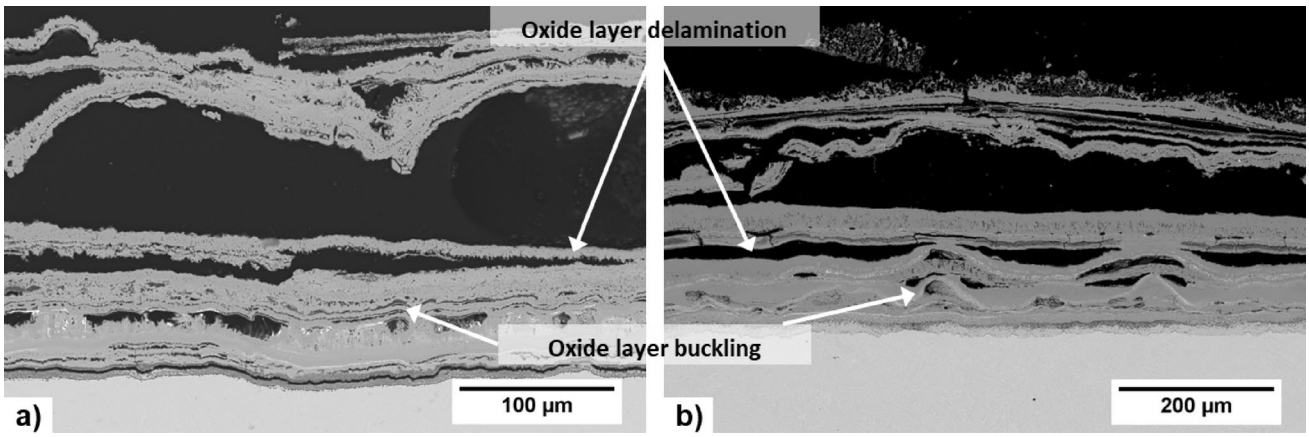


Fig. 7 FESEM cross-section image of uncoated SVM12 after: **a** 1000 h and **b** 2000 h of exposure to a model biomass corrosion atmosphere at 600 °C with KCl deposits

developed, and spallation was evident upon visual inspection of the sample. The image reveals buckling and partial detachment of the scale, likely caused by stresses generated during the growth of different oxides. Indeed, EDS mapping shows Cr and Fe-rich oxides, as well as internal oxidation within the substrate (Fig. 8). The Cr content varied significantly, ranging from 5 to 40 wt%, with the highest content located mostly at the interface with the substrate. Other minor elements present in the SVM12 alloy, such as Mn and Si, were also found in the oxide scales at lower concentrations (≈ 0.5–1 wt% in both cases). This suggests that these elements also diffuse outwards, and it is very likely that outwards-growing pure Fe oxides form but spall easily, which would explain why they were not clearly observed. The corresponding XRD pattern shown in Fig. 9 mainly indicates the presence of Fe_2O_3 as well as some very low-intensity peaks that can be attributed to Fe,Cr spinel (other peaks overlap with those attributed to Fe_2O_3), in agreement with the presence of Cr at the outer surface (Cr: 11 wt%). The oxide scale continued to grow with prolonged exposure, as evidenced by the image shown in Fig. 7b, showing the cross-section of the sample taken after 2000 h. The remaining scale retains a similar morphology and composition to that obtained after 1000 h, but is much thicker, with additional buckling and extensive de-cohesion. In the sample exposed for 8000 h (Fig. 10), three more compact and distinct layers are observed, with the top one containing Cr only at the interface with the subsequent layer, which appears detached in Fig. 8. This layer exhibits thick cracks

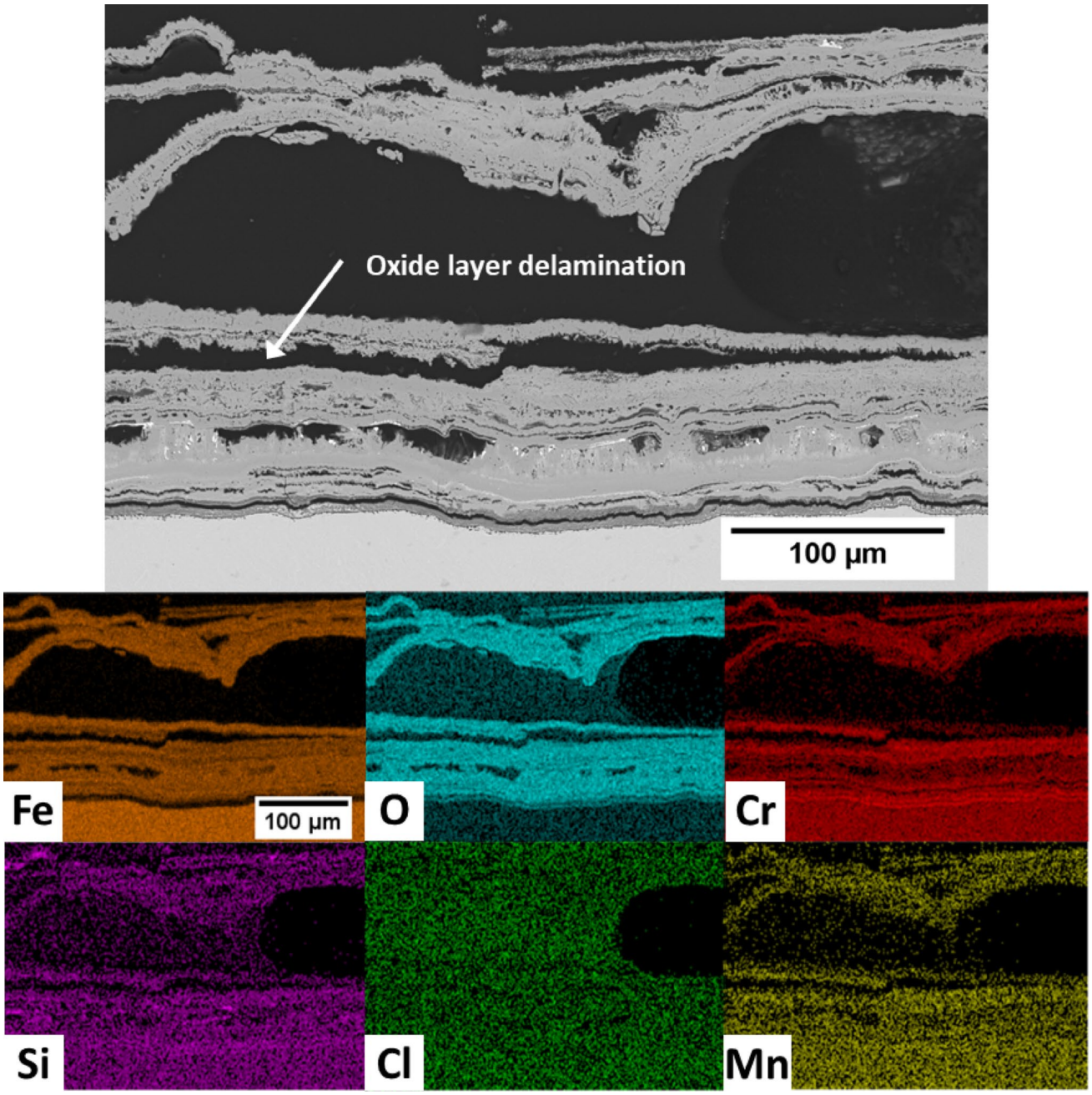


Fig. 8 FESEM element mapping of the uncoated SVM12 after 1000 h of exposure to a model biomass corrosion atmosphere at 600 °C with KCl deposits

perpendicular to the surface and matches Fe_2O_3, as confirmed by the corresponding peaks in the XRD pattern (Fig. 11). The presence of a relatively Cr-rich zone in between this outer zone and the next one, may be explained by the slow outward diffusion of Cr at 600 °C. Peaks corresponding to Cr, Fe spinels are also visible in the XRD pattern shown in Fig. 11. The subsequent layer is very likely $(Fe, Cr)_3O_4$, containing varying amounts of Cr, as evidenced by the presence of Cr-rich bands typical of this spinel. Quaddakkers and collaborators have seen similar results in ferritic steels and attribute it to the repetition of cycles in which Cr-rich spinels form due to rapid Cr diffusion from the bulk alloy. However, this spinel cannot be sustained due to continuous depletion as Cr continues to diffuse outwards, which results in the formation

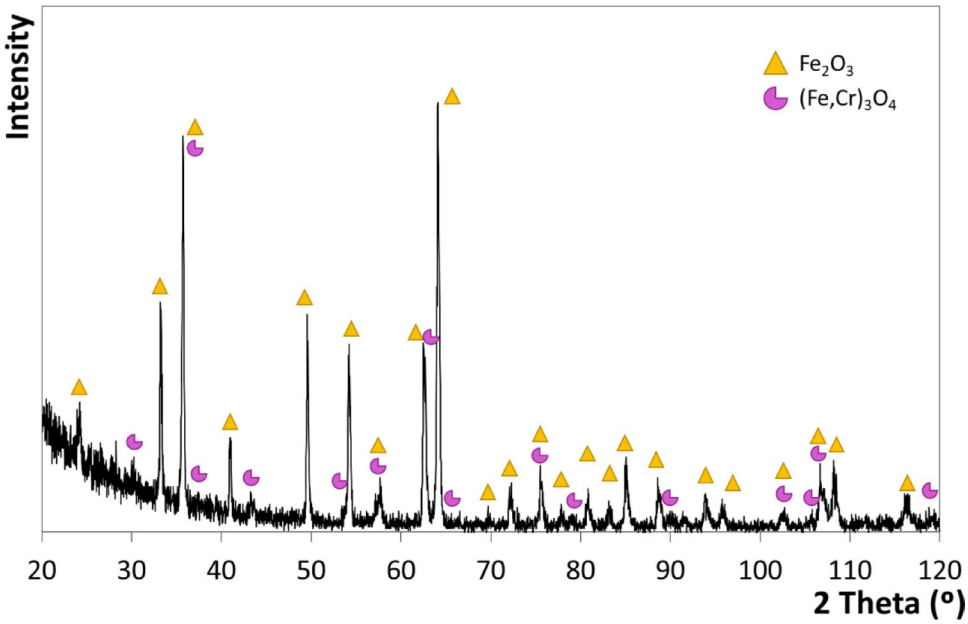


Fig. 9 XRD pattern of uncoated SVM12 after 1000 h of exposure to a model biomass corrosion atmosphere at 600 °C with KCl deposits

of Fe-rich spinels [21]. Moreover, at the interface between the spinel layer and the third, innermost Cr-rich zone, a thin Si- and W-rich film is observed. These two elements are present in the substrate and could potentially act as markers, showing where the original surface is located, delimitating the outward-growing scale developed, which is primarily due to Fe outwards diffusion. It is worth noting that W diffusion is extremely slow at 600 °C. As mentioned, this also implies that some Cr has diffused outwards after such a long exposure (8000 h). Cr was also detected in the outer scale of other ferritic steels (EN1.4021 and EN1.4057) with higher Cr content (≈20wt %) than SVM12 (≈11wt %) [22]. The inward-growing Cr-rich Fe, Cr spinel constitutes the third and innermost scale zone. Some Cr depletion below this zone is actually observed in the elemental mapping shown in Fig. 10. These three phases, as well as similar scale morphologies, have also been observed by other research groups when exposing other ferritic steels to similar conditions [23, 24].

SHS coating without Al

After exposure to the biomass model conditions at 600 °C for 2000 h, the Al-free SHS coating shows significant corrosion, forming a thick, dense, outer-growing oxide rich in Fe and Cr, with a thickness of 60–70 µm, which appears to be easily detached, as shown in Fig. 12. Two different zones can be observed within this oxide: the inner zone is rich in Cr and contains some Mn, whereas the outermost layer consists predominantly of Fe oxide with very low Cr content. Below the oxide, within the original coating, three distinct zones can be observed (Fig. 13). Inside the outermost region (zone I), extensive internal oxidation of the coating is evident, and also Cr depletion (≈ 2 wt% Cr) within unoxidized Fe-rich "strings", corresponding to the remnants of the original coating splats, embedded in a Cr-rich oxide. Beneath this, in zone II, which is also Cr-depleted, oxidation and a very high level of porosity are observed. Eklund and collaborators observed oxidation along splat boundaries in a NiCr coating deposited by HVAF, exposed to KCl at 600 °C for 168 h, resulting in the formation of voids, as splats are separated causing the boundaries to widen [17]. Pidcock and coworkers [14] also observed depletion layers in HVOF deposited coatings, accompanied by an apparent increase in porosity. Finally, zone III in contact with the substrate, seems to be the remaining un-attacked coating. According to EDX analysis, this zone maintains its original composition. Zone III is absent in some areas, indicating total coating degradation, whereas it reaches a maximum of 25 µm in others. Considering the initial coating thickness of 200 µm, this implies a very high rate of degradation which may be explained by the reaction of KCl with Cr-oxide as observed by others, to generate K_2CrO_4 [25]. Significant amounts of Cl were detected at the surface and extending to the coating-substrate interface, similarly to Eklund's observations on NiCr coatings [17]. The XRD pattern displayed peaks that can also be attributed to Fe_2O_3 which correspond to the outermost layer observed in this sample, as well as some other peaks that match $(Fe, Cr)_3O_4$. No peaks corresponding to the coating can be observed (Fig. 14).

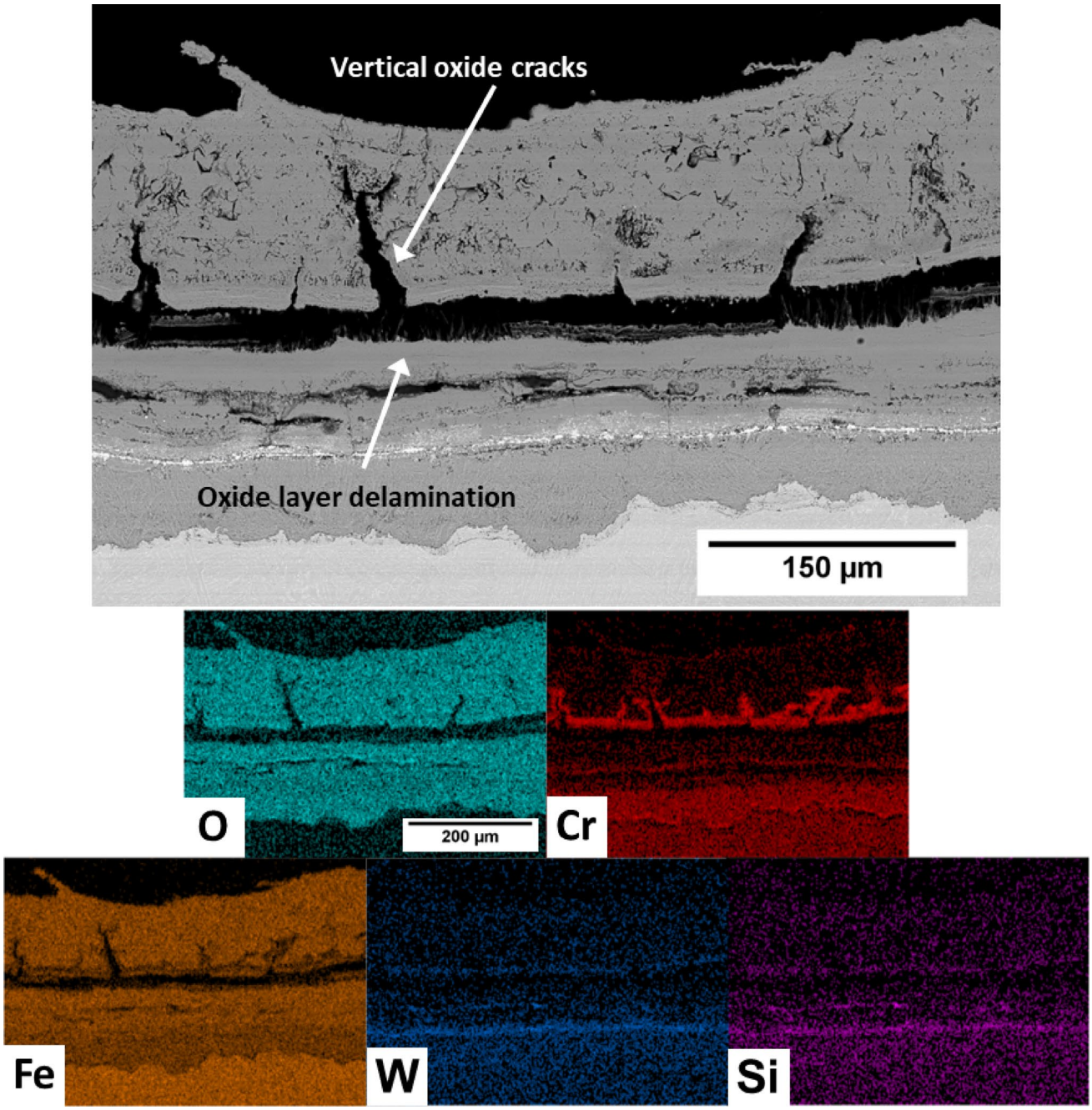


Fig. 10 FESEM cross-sectional and element mapping images of uncoated SVM12 after 8000 h of exposure to a model biomass corrosion atmosphere at 600 °C with KCl deposits

Al modified SHS coating

The Al-modified SHS coating exposed for 2000 h at 600 °C to the model biomass atmosphere, exhibited some corrosion products forming a porous, irregular and incoherent oxide scale (Fig. 15), apparently present only in some regions, on top of a thin and denser oxide which completely covers the surface of the coating (Fig. 16). The thicker oxide layer is highly enriched in Al, containing minimal amounts of Fe and Cr (< 1 wt%) as well as 3 wt% of K and 1 wt% of Cl. Its maximum thickness reaches approximately 40 µm in some areas, as shown on Figs. 15 and 16. The thinner scale is rich in Al and Cr with some Fe content, also containing small amounts of K. The XRD pattern exhibited in Fig. 17, shows

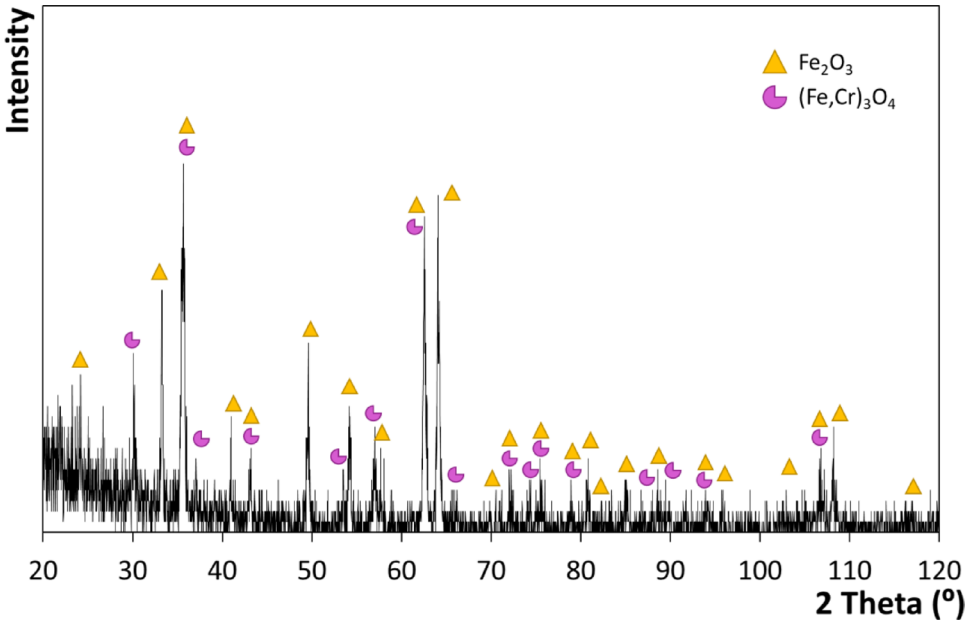


Fig. 11 XRD pattern of uncoated SVM12 after 8000 h of exposure to a model biomass corrosion atmosphere at 600 °C with KCl deposits

peaks attributed to Fe_2O_3, $(Fe, Cr)_3O_4$ and α-Al_2O_3 as well as the coating phase (α-FeCr). The formation of α-Al_2O_3 at this low-temperature has previously been observed in our laboratory for slurry aluminide coatings exposed to the same biomass model atmosphere [18]. However, in this case, we believe that this oxide was already present prior to exposure, formed during the coating heat treatment process, and has subsequently grown in thickness. Notably, Cl and K were not detected within the coating, in contrast to the Al-free SHS coating, in which as mentioned, these corrosive species reached the substrate. The coating exhibits some further Al oxide growth internally (at the splat boundaries), again where Al oxide was observed initially (as seen in Figs. 4 and 5), but it is now significantly thicker. In addition, Al depletion was observed at the surface to a depth of ≈ 50 µm, likely due to the formation of the thick Al oxide observed on top of the coating (Figs. 15 and 16). Eklund and coworkers also observed internal Al oxide formation in NiAl coatings in contact with KCl at 600 °C [17]. On the contrary, and as opposed to the Al-free coating, hardly any Cr depletion, or the development of pores can be observed. Clearly, coating degradation is significantly slower in the Al-enriched coating as its original thickness remains largely intact, and little Cr and/or Fe are consumed to develop the corrosion products. Within the rest of the coating, Al continues to interdiffuse with the coating material within the splats. For instance, EDS point analysis provided a composition of 5 wt% Al and 23 wt% Cr at the spot marked on Fig. 16.

After 8000 h of exposure, the Al-enriched coating is still very protective with no evidence of substrate attack. However, a higher degree of coating degradation is observed with outer growing oxides that can reach > 100 µm in thickness (Fig. 18). This oxide is "spongy", poorly coherent (Fig. 19) and likely has spalled in some spots. It is rich in Al, Fe and also contains some Cr. The thin, continuous oxide observed on the coating's surface exposed for 2000 h is still present and again contains Al, Cr and small amounts of Fe. Oxidation at splat boundaries has become quite substantial, reaching deeper into the coating (up to 100–150 µm) and maintaining a similar morphology to that observed in the sample exposed for 2000 h, but with further growth of the Al-rich oxide at the splat boundaries (Fig. 20). In the same figure, it can be seen how the coating is Al depleted in the internal oxidation zones whereas in the un-attacked coating Al interdiffusion continued, and element mapping illustrates how its distribution is further homogenized. Despite the increment in internal boundary oxidation, there was no apparent coating thickness loss, very little Cr depletion and no porosity development is observed, confirming the high corrosion resistance provided by this coating. The XRD pattern shown in Fig. 21 confirms the presence of α-Al_2O_3 as well as Fe_2O_3 with the peaks corresponding to α-Al_2O_3 being more intense. No coating peaks could be observed likely due to the corrosion products thickness.

Discussion

The corrosion resistance of the Al-modified SHS coating appears to be significantly higher than the Al-free SHS coating under the testing conditions employed. After 2000 h of exposure, the thickness of the corrosion products developed

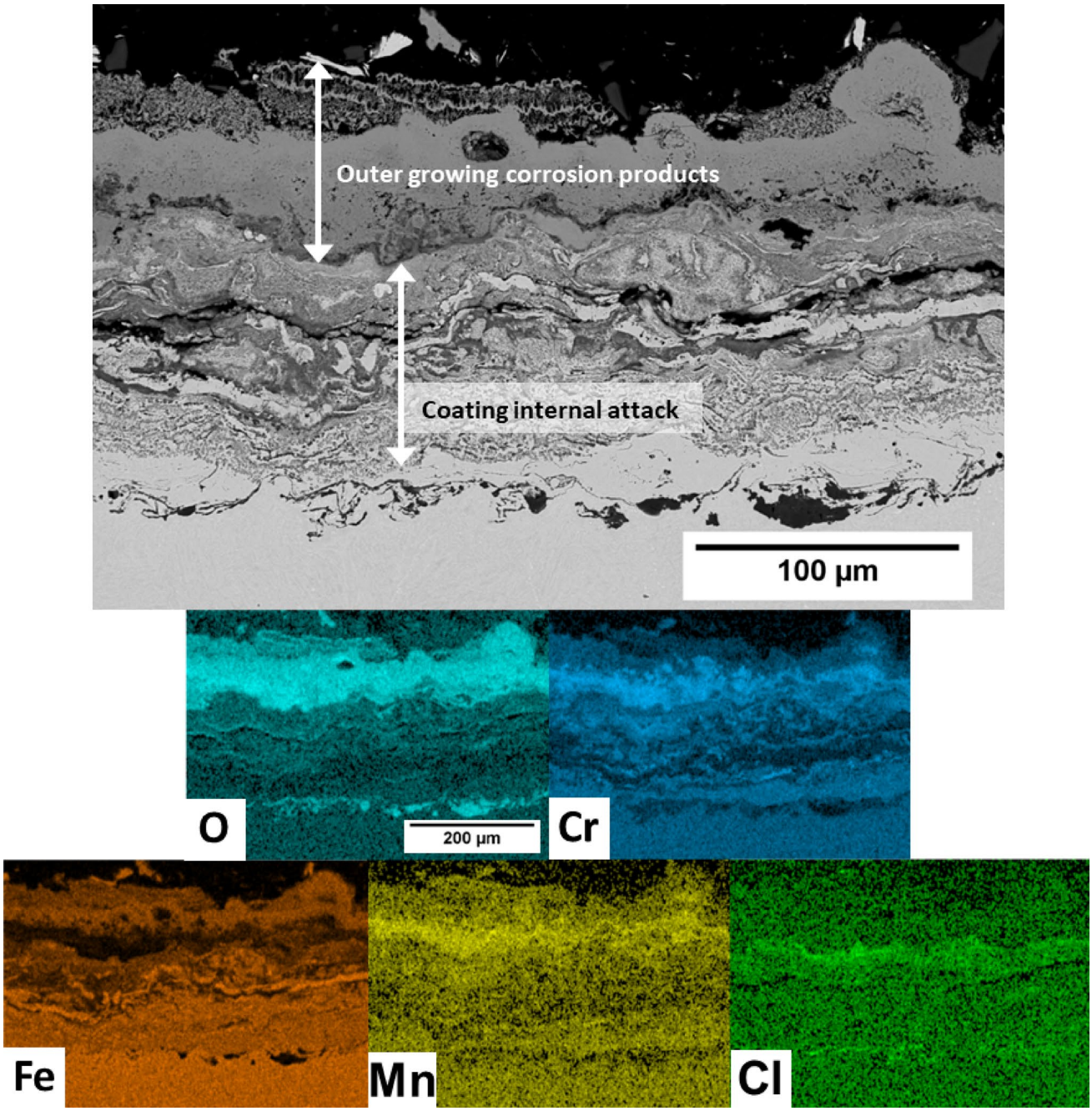


Fig. 12 FESEM cross-sectional and element mapping images of the SHS coating after 2000 h of exposure to a model biomass corrosion atmosphere at 600 °C with KCl deposits

on the unmodified SHS coating was within the range of 60–80 µm and the depth affected by internal oxidation in the remaining coating measured approximately 75–100 µm, whereas in the Al-modified SHS coating after the same exposure, 5–40 µm of corrosion products were observed on top of the coating, which exhibited very little attack, with essentially alumina formation in the inter-splat boundaries closed to the coating surface. However, Sadeghimeresh and collaborators found that Al has a negative effect on biomass corrosion when exploring the behaviour of MCrAlY coatings in the presence of a model biomass atmosphere including KCl deposits at 600 °C [26]. They observed voids at

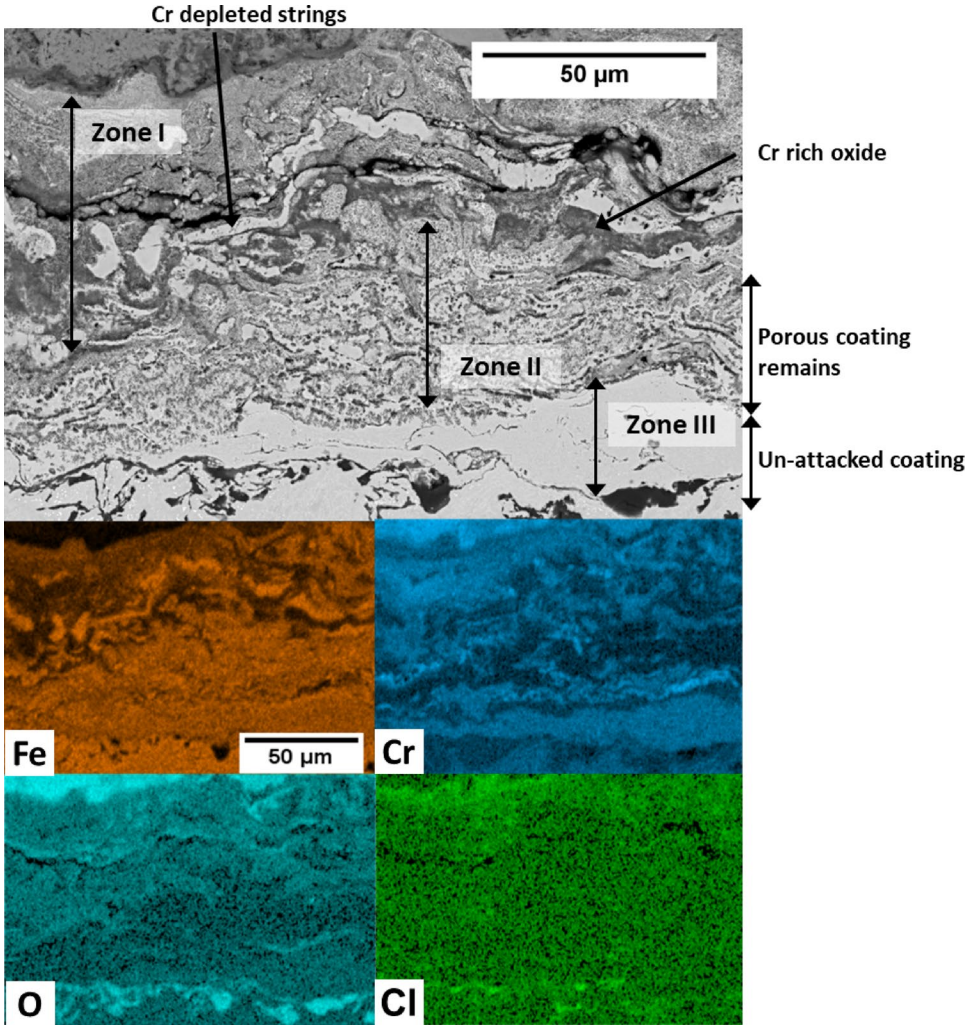


Fig. 13 Higher magnification FESEM cross-sectional and element mapping image s of the remains of the SHS coating after 2000 h of exposure under a model biomass corrosion atmosphere at 600 °C with KCl deposits

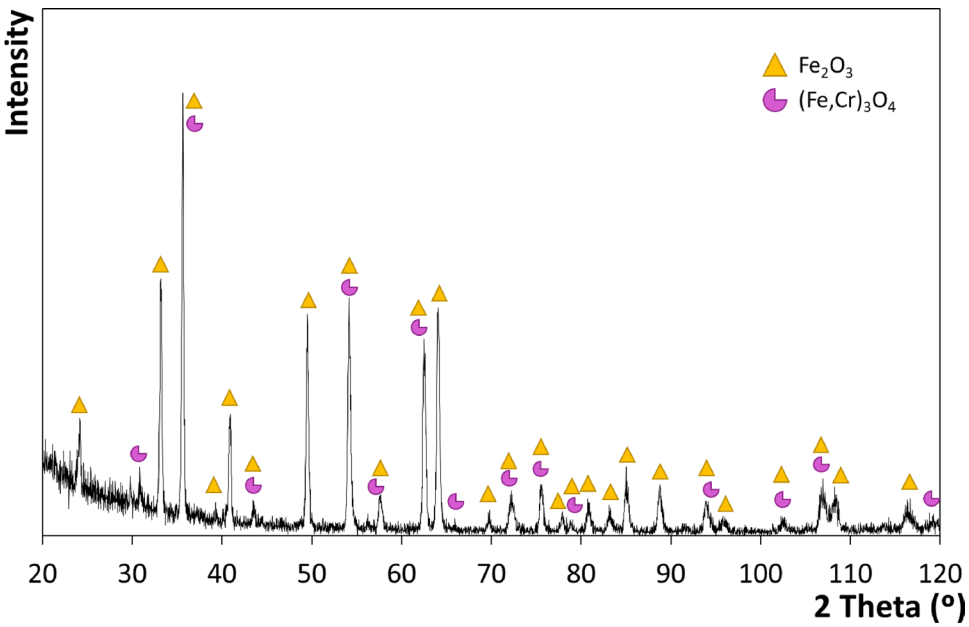


Fig. 14 XRD pattern of SHS coating after 2000 h of exposure to a model biomass corrosion atmosphere at 600 °C with KCl deposits

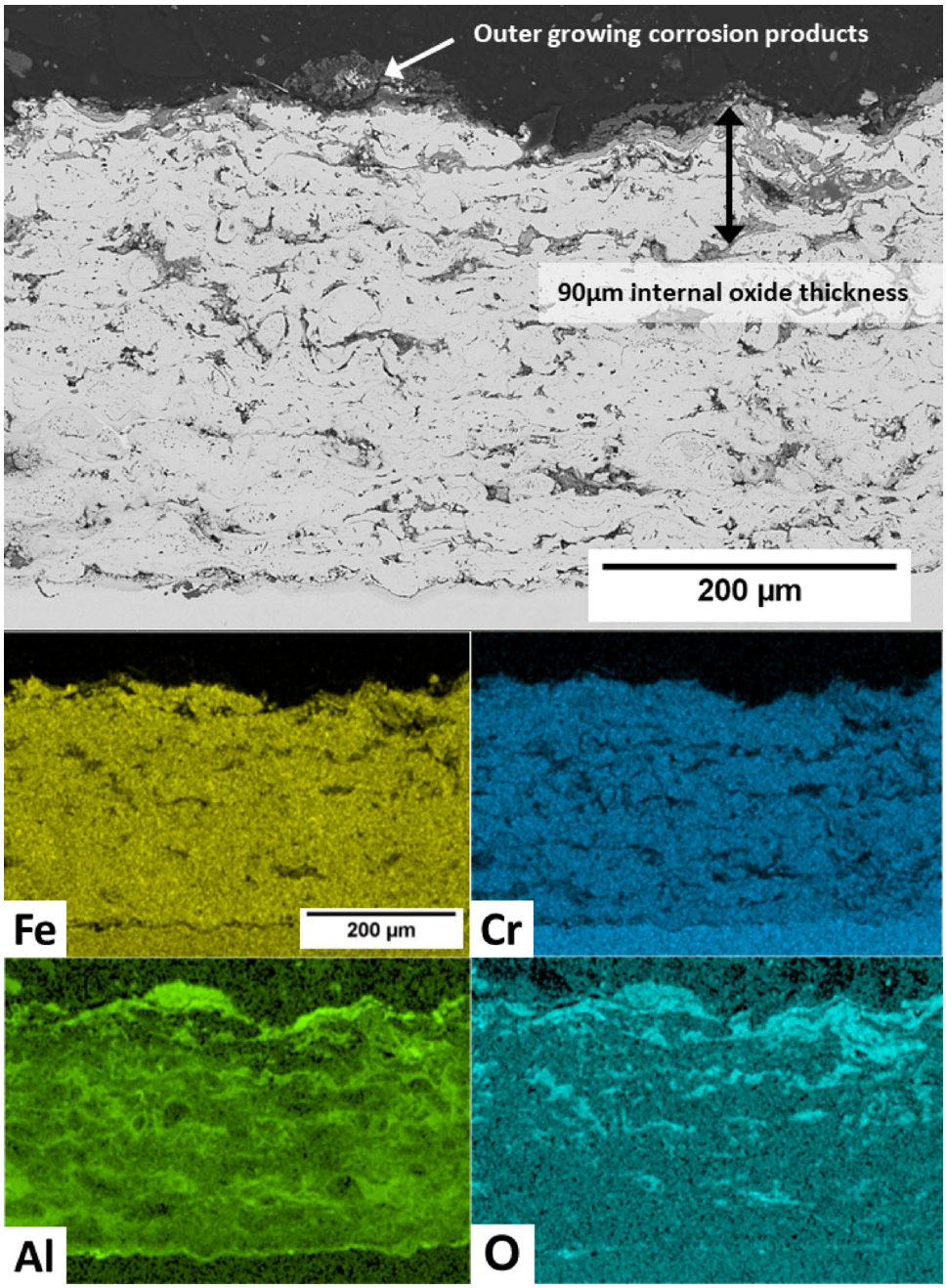


Fig. 15 FESEM cross-sectional and element mapping images of the Al-modified SHS coating after 2000 h of exposure to a model biomass corrosion atmosphere at 600 °C with KCl deposits

the external coating zones, along with oxidation and Al depletion after only 168 h of exposure. This was attributed to the formation of volatile Al and Cr chlorides. As previously mentioned, our laboratory has also found that Al-rich diffusion coatings are not highly resistant to biomass corrosion. Specifically, a slurry aluminide coating deposited also on SVM12, was exposed to the same conditions used in the present work, and a very thick, non-protective and non-dense α-Al_2O_3 developed rapidly, depleting the coating from Al [19]. On the contrary, Sadeghimeresh and collaborators [27] as well as Jafari et al. [28], found that HVAF sprayed Ni5Al coatings were not attacked by KCl and did not show internal oxidation, due to the formation of a continuous and protective oxide scale according to the authors.

Possible, non-exclusive explanations of the beneficial effect of Al in the coating observed in the present study may be related to: (a) the significant reduction of coating porosity (≅ 8% according to ImageJ) which hinders the

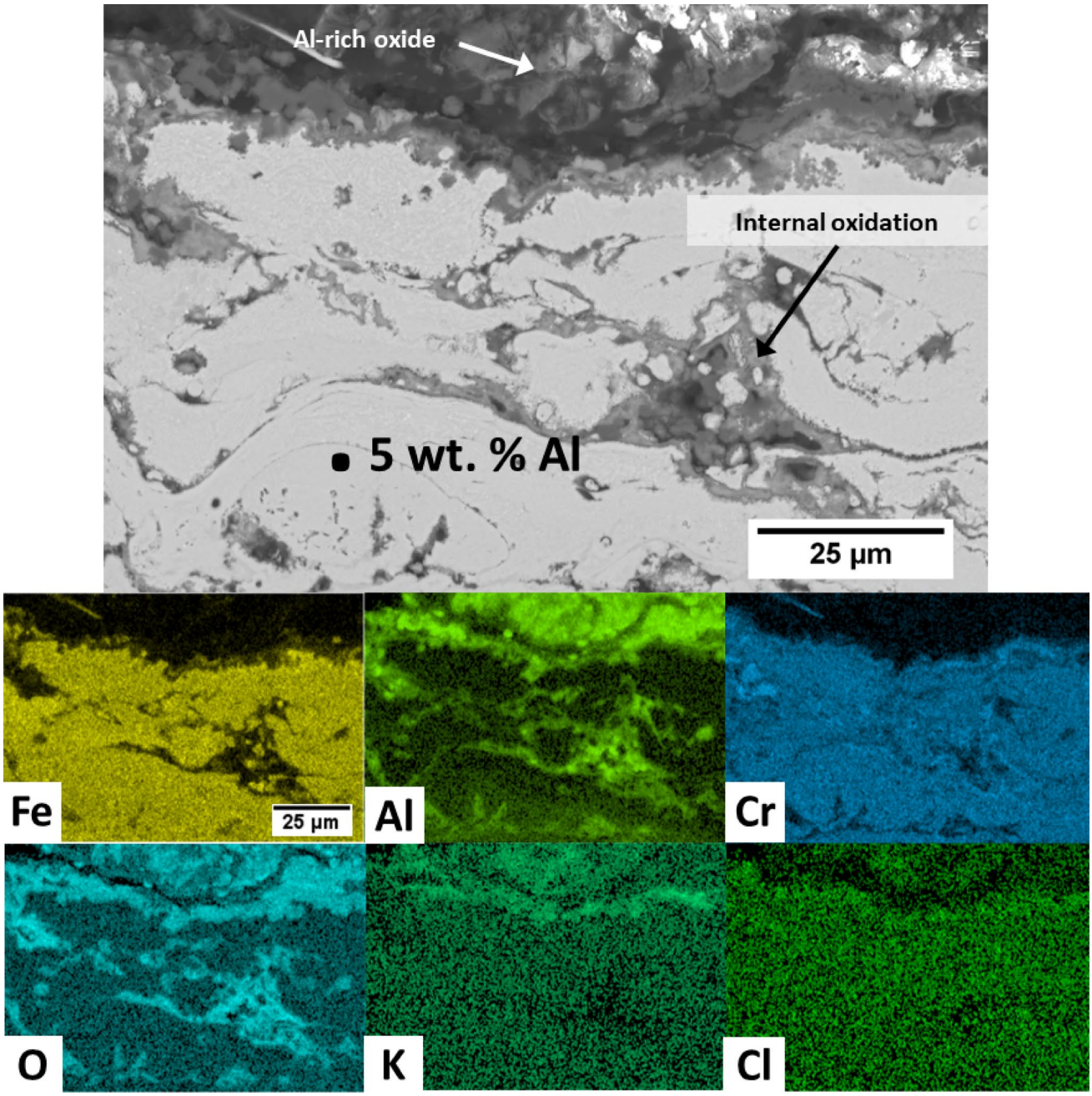


Fig. 16 FESEM cross-sectional and element mapping images of the near-surface zone of the Al-modified SHS coating after 2000 h of exposure to a model biomass corrosion atmosphere at 600 °C with KCl deposits

penetration of the corrosive species into the coating, (b) the presence of Fe-Al intermetalics which exhibit higher corrosion resistance than FeCr alloys and (c) the formation of relatively protective Al oxide within the splat boundaries prior to exposure (Fig. 4) as this oxide grows over time, and further blocks or hinders the access of Cl-containing species. Indeed, the reaction of α-Al_2O_3 with KCl is not thermodynamically favoured [25], so it can act as a barrier to prevent the reaction of Fe, Cr and/or Al with Cl-containing species.

$$Al_2O_3\,(s) + 2KCl\,(s) + \tfrac{1}{2}O_2 \rightarrow 2KAlO_2\,(s) + 2Cl_2\,(g)$$

$$\Delta G_f^0 = 1122,5 \tfrac{kJ}{mol} \text{ at } 600\,^{\circ}C \text{ [24]}$$

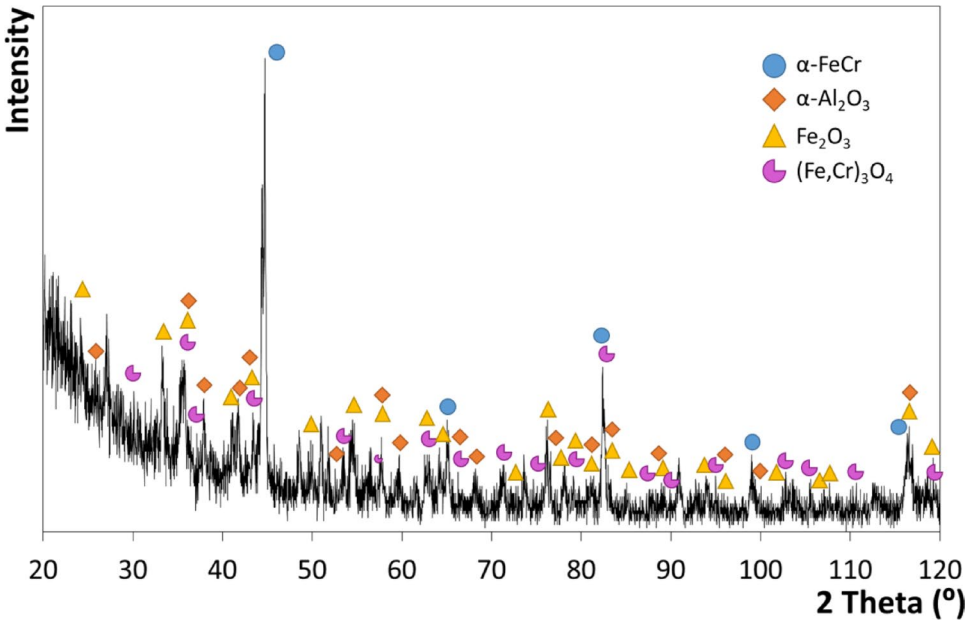


Fig. 17 XRD pattern of Al-modified SHS coating after 2000 h of exposure to a model biomass corrosion atmosphere at 600 °C with KCl deposits

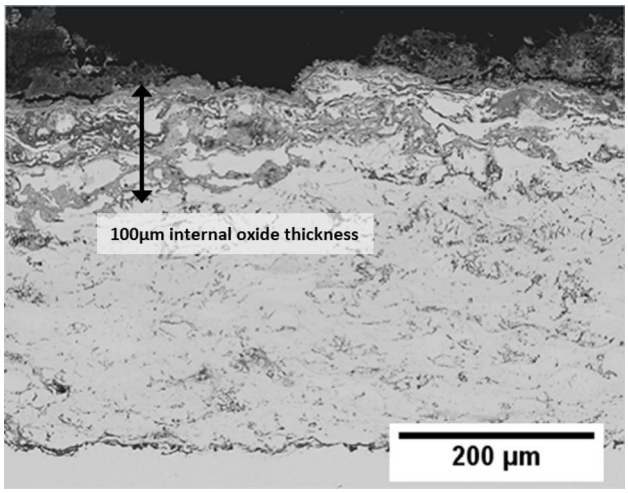


Fig. 18 FESEM cross-section of Al-modified SHS coating after 8000 h of exposure at a model biomass corrosion atmosphere at 600 °C with KCl deposits

This is supported by the results obtained by other research groups. For instance, Fantozzi and collaborators [29], exposed self-standing thermally sprayed Al_2O_3-40ZrO_2, (after removing the substrate) in contact with KCl at 720 °C and no degradation was observed after 72 h, whereas Cr_2O_3-based coatings were severely attacked by KCl, even at lower temperatures forming K_2CrO_4. In addition, Luo et al. exposed yttria stabilized zirconia (YSZ) with an Al_2O_3 overlay to a molten NaCl-KCl eutectic at 750 °C for 12 h, and no degradation was observed in the Al_2O_3 layer whilst the YSZ was corroded [30].

Several authors propose that a low-melting eutectic can be formed by mixing KCl and K_2CrO_4 which in turn can dissolve Cr_2O_3 [31, 32]. Unfortunately, when Al_2O_3-40ZrO_2 was tested as a coating on steel S235, it detached.

The Al-free SHS coating suffers from severe Cr depletion due to the formation of non-protective Fe and Cr oxides, likely because it reacts with KCl. As a result, voids are generated, and through them, the access of the corrosive species enhances the degradation process. But when Al is present at the grain boundaries and Al oxide forms before exposure, this oxide hinders the attack of the corrosive species preventing reaction with the steel coating. Over time, the oxide grows slowly, depleting the metallic splats from Al, but these Al-containing scales continue to act as a barrier to K and Cl corrosive species. Although oxidation still progresses deeper into the coating, it only advanced from a maximum of 85 µm at 2000 h to ≅ 100 µm after 8000 h indicating a slow advance. Therefore, access for larger corrosive species to penetrate the coating and reach the substrate seems to be hampered.

The Al-modified SHS demonstrated superior corrosion resistance after 8000 h of laboratory exposure to a biomass corrosion model atmosphere. To the best of our knowledge, there are no published results of such a long-term exposure in the laboratory. Some coatings have been tested in operating plants for longer periods (up to 3 years) but at lower temperatures, never surpassing 540 °C [8].

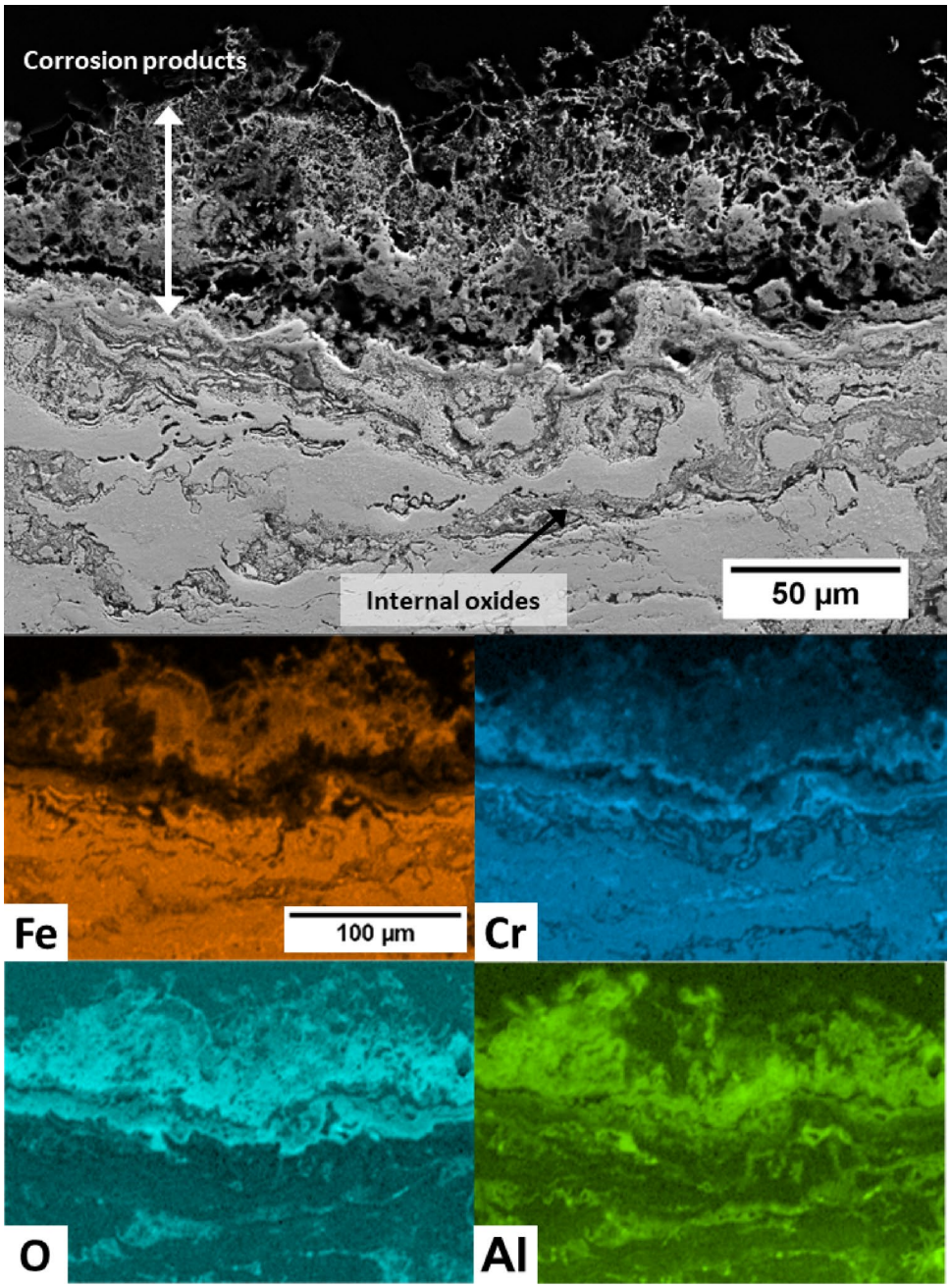


Fig. 19 FESEM cross-section and element mapping of the surface zone of the Al-modified SHS coating after 8000 h of exposure at a model biomass corrosion atmosphere at 600 °C with KCl deposits

Conclusions

A new Al-modified high hardness steel coating was developed and applied by HVOF, and its performance against biomass-induced corrosion was evaluated at 600 °C over a period of 8000 h. The presence of Al within the coating significantly enhanced its resistance to biomass corrosion when compared to the uncoated SVM12 and unmodified SHS coating. After heat treatment prior to exposure to the biomass combustion model atmosphere, the coating exhibited a modest degree of internal oxidation at the splat boundaries, resulting in the formation of Al oxide. The unmodified SHS coating offered some degree of protection, behaving better that uncoated SVM12, but demonstrated substantially

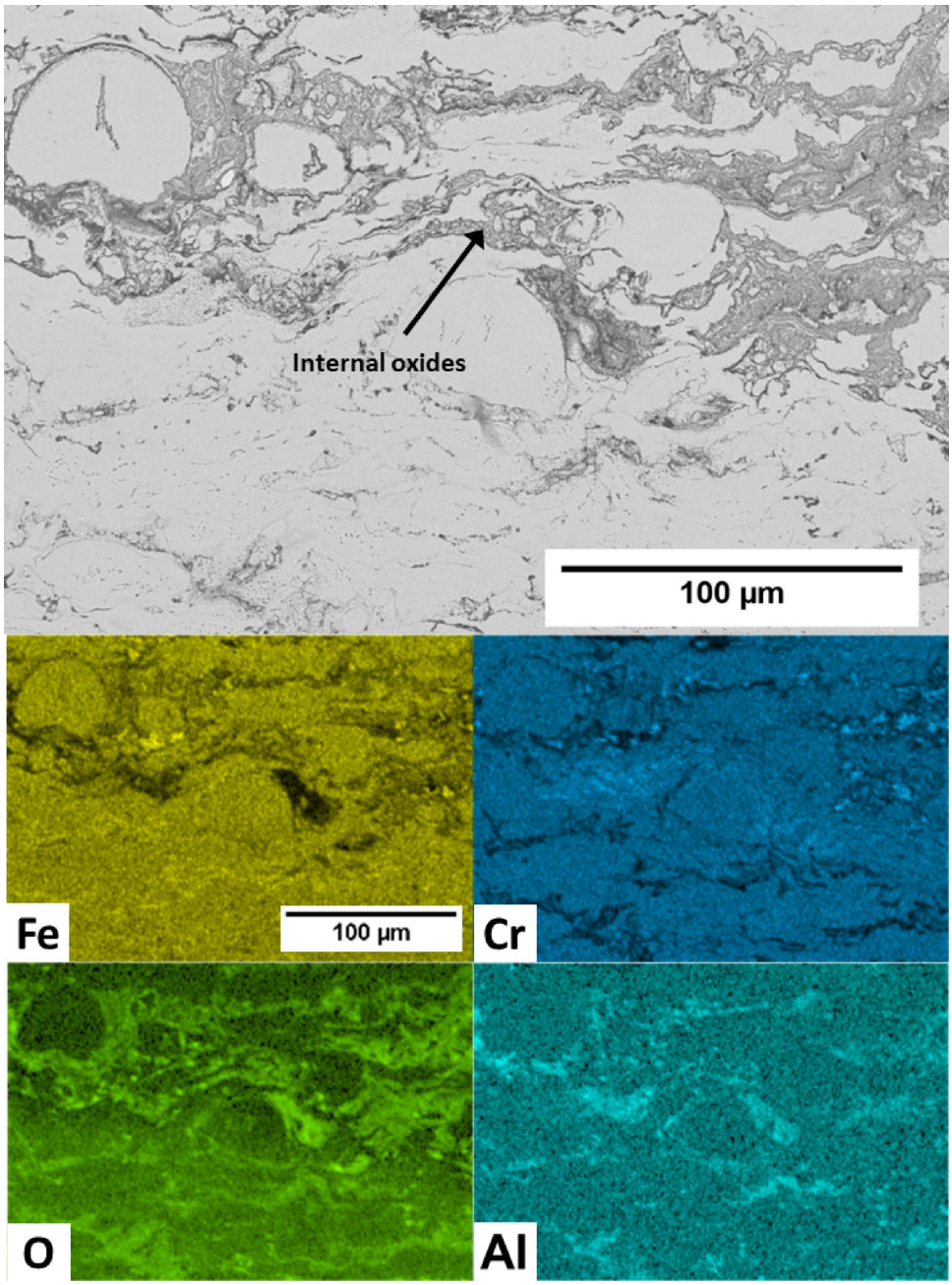


Fig. 20 Detailed observation of the Al-modified SHS coating at the boundary between the internal oxidation zone and the un-attacked coating after 8000 h of exposure at a model biomass corrosion atmosphere at 600 °C with KCl deposits: FESEM cross-section and element mapping

inferior corrosion resistance after only 2000 h of exposure relative to the Al-modified coating, suffering significant degradation by internal oxidation and Cr depletion. As a result, thick Fe and Cr oxides scales developed and a considerable degree of porosity formed within the coating.

Possible reasons for the improved behaviour of the Al-modified coating are the porosity reduction and the presence of FeAl intermetallics and Al oxide within the splat boundaries prior to exposure to the corrosive atmosphere. This Al oxide likely offers two protection mechanisms: (a) it prevents the reaction of the coating's metallic components with Cl-containing species, as Al oxide is not attacked by these species and (b) it hinders the penetration of Cl corrosive species by blocking their pathways along splat boundaries.

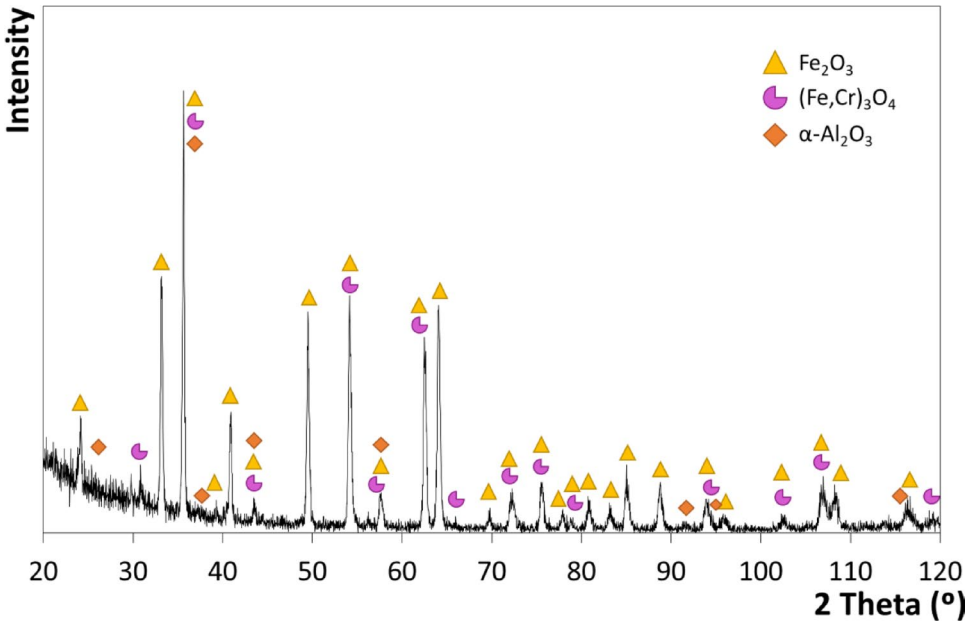


Fig. 21 XRD pattern of Al-modified SHS coating after 8000 h of exposure at a model biomass corrosion atmosphere at 600 °C with KCl deposits

Acknowledgements The authors thank all the members of the Metallic Materials Area at INTA for technical support.

Authors contribution Alina Agüero: Conceptualization; Methodology; Project administration; Supervision; Writing—original draft; Writing—review & editing. Marcos Gutiérrez: Conceptualization; Investigation; Validation; Writing—review & editing. Pauline Audigié: Conceptualization; Investigation; Methodology; Validation; Writing—review & editing. Sergio Rodríguez: Investigation; Validation. Jon Pascual: Investigation; Validation.

Funding This project has received funding from the European Union's Horizon 2020 research and innovation program under Grant Agreement No. 815147 (BELENUS project).

Data availability The test data that support the findings of this study are available from the corresponding authors upon reasonable request.

Declarations

Conflict of interest The authors have no competing interests to declare that are relevant to the content of this article.

Open Access This article is licensed under a Creative Commons Attribution 4.0 International License, which permits use, sharing, adaptation, distribution and reproduction in any medium or format, as long as you give appropriate credit to the original author(s) and the source, provide a link to the Creative Commons licence, and indicate if changes were made. The images or other third party material in this article are included in the article's Creative Commons licence, unless indicated otherwise in a credit line to the material. If material is not included in the article's Creative Commons licence and your intended use is not permitted by statutory regulation or exceeds the permitted use, you will need to obtain permission directly from the copyright holder. To view a copy of this licence, visit http://creativecommons.org/licenses/by/4.0/.

References

1. Majamo, S.L., Amibo, T.A., Bedru, T.K.: Synthesis and application of biomass-derived magnetic biochar catalyst for simultaneous esterification and trans-esterification of waste cooking oil into biodiesel: modeling and optimization. Mater. Renew. Sustain. Energy **12**, 147–158 (2023). https://doi.org/10.1007/s40243-023-00236-5
2. Sugebo, B.: A review on enhanced biofuel production from coffee by-products using different enhancement techniques. Mater. Renew. Sustain. Energy **11**, 91–103 (2022). https://doi.org/10.1007/s40243-022-00209-0
3. Gill, T., Birch, T.: A guide to biomass power plants, The Eco-experts, A guide to biomass power plants | The Eco Experts. Accessed 31 July 2025
4. Bulkowska, K., Mriusz Gusiatin, Z., Klimiuk, E., Pawlowski, A., Pokoj, T.: Biomass for Biofuels. CRC Press/Balkema, Taylor & Francis Group, London, UK. (ISBN: 978–1–138–02631–5)
5. Wu, D.L., Dahl, K.V., Christiansen, T.L., Montgomery, M., Hald, J.: Corrosion behaviour of Ni and nickel aluminide coatings exposed in a biomass fired power plant for two years. Surf. Coat. Technol. **362**, 355–365 (2019). https://doi.org/10.1016/j.surfcoat.2018.12.129
6. Karlsson, S., Pettersson, J., Johansson, L.-G., Svensson, J.E.: Alkali induced high temperature corrosion of stainless steel: the influence of NaCl, KCl and $CaCl_2$. Oxid. Met. **78**, 83–102 (2012). https://doi.org/10.1007/s11085-012-9293-7
7. Shower, P.: Corrosion and Erosion Coatings for Biomass (Combustion) with load following. Proceedings of 2023 FECM/NETL Spring, Pittsburg, PA, R&D Project Meeting, April (2023). https://netl.doe.gov/sites/default/files/netl-file/23FECM_19_Shower.pdf. Accessed 07 May 2025
8. Kawahara, Y.: An overview on corrosion-resistant coating technologies in biomass/waste-to-energy plants in recent decades. Coatings **6**, 34 (2016). https://doi.org/10.3390/coatings6030034
9. Kish, J.R., Reid, C., Singbeil, D.L., Seguin, R.: Corrosion of high-alloy superheater tubes in a coastal biomass power boiler. Corrosion **64**(4), 356–366 (2008). https://doi.org/10.5006/1.3278479

10. Agüero, A., Muelas, R., González, V.: HVOF coatings for steam oxidation protection. Mater. Corros. **59**, 393–401 (2008). https://doi.org/10.1002/maco.200804121
11. Agüero, A., Gutiérrez, M., Muelas, R., Plana, D., Román, A., Hernández, M.: Laboratory corrosion testing of coatings and substrates simulating coal combustion under a low NOx burners atmosphere. Mater. Corros. **65**, 149–160 (2014). https://doi.org/10.1002/maco.201307096
12. Sadeghi, E., Markocsan, N., Joshi, S.: Advances in corrosion-resistant thermal spray coatings for renewable energy power plants. Part I: effect of composition and microstructure. J. Therm. Spray Technol. **28**, 1749–1788 (2019). https://doi.org/10.1007/s11666-019-00938-1
13. Agüero, A., Baráibar, I., Gutiérrez, M., Hernández, M., Muelas, R., Rodríguez, S.: Biomass corrosion behavior of steels and coatings in contact with KCl/K_2SO_4 at 550°C under an oxy-fuel combustion atmosphere: a screening laboratory test. Surf. Coat. Technol. **350**, 188–200 (2018). https://doi.org/10.1016/j.surfcoat.2018.05.082
14. Pidcock, A., Mori, S., Sumner, J., Simms, N., Nicholls, J., Oakey, J.: High temperature corrosion of HVOF coatings in laboratory-simulated biomass combustion superheater environments. Oxid. Met. **99**, 101–115 (2023). https://doi.org/10.1007/s11085-022-10141-3
15. Bai, M., Reddy, L., Hussain, T.: Experimental and thermodynamic investigations on the chlorine-induced corrosion of HVOF thermal sprayed NiAl coatings and 304 stainless steels at 700 °C. Corros. Sci. **135**, 147–157 (2018). https://doi.org/10.1016/j.corsci.2018.02.047
16. Abu-warda, N., Tomás, L.M., López, A.J., Utrilla, M.V.: High temperature corrosion behavior of Ni and Co base HVOF coatings exposed to NaCl-KCl salt mixture. Surf. Coat. Technol. **418**, 127277 (2021). https://doi.org/10.1016/j.surfcoat.2021.127277
17. Eklund, J., Phother, J., Sadeghi, E., Joshi, S., Liske, L.: High-temperature corrosion of HVAF-sprayed Ni-based coatings for boiler applications. Oxid. Met. **91**, 729–747 (2019). https://doi.org/10.1007/s11085-019-09906-0
18. European Commission project "Lowering Costs by Improving Efficiencies in Biomass Fueled Boilers: New Materials and Coatings to Reduce Corrosion- BELENUS", 2019–2024, https://belenus-project.eu/. Accessed 07 May 2025
19. Agüero, A., Audigié, P., Rodríguez, S., Gutiérrez, M., Pascual, J., Ssenteza, V., Jonsson, T., Johansson, L.-G.: Rapid α-Al_2O_3 growth on an iron aluminide coating at 600 °C in the presence of O_2, H_2O, and KCl. ACS Appl. Mater. Interfaces **16**, 59507–59515 (2024). https://doi.org/10.1021/acsami.4c11719
20. WEARTECH SHS800HV HVOF Hardfacing - Severe Abrasion Thermal Spray Powder https://chdelivery.lincolnelectric.com/api/public/content/c580ff61450f49fc9c7059f97ade3942?v=365ee1ae. Accessed 07 May 2025
21. Quadakkers W. J., Ennis, P. J.: Materials for Advanced Power Engineering 1998. In: J. Lecomte-Beckers et al. (Eds) pp. 123–138. Forschungszentrum Julich Gmbh, Germany (1998)
22. Kiamehr, S., Dahl, K.V., Montgomery, M., Somers, M.A.J.: KCl-induced high temperature corrosion of selected commercial alloys Part I: chromia-formers. Mater. Corros. **66**, 1414–1429 (2015). https://doi.org/10.1002/maco.201408213
23. Olivas-Ogaz, M.A., Eklund, J., Persdotter, A., et al.: The influence of oxide-scale microstructure on KCl(s)-induced corrosion of low-alloyed steel at 400 °C. Oxid. Met. **91**, 291–310 (2019). https://doi.org/10.1007/s11085-018-9881-2
24. Dudziak, T., Hussain, T., Orlicka, D., Pokrywa, A., Simms, N.J.: Fireside corrosion degradation of 15Mo3, T22, T23 & T91 in simulated coal-biomass co-fired environment. Mater. Corros. **66**, 839–850 (2015). https://doi.org/10.1002/maco.201407886
25. Meissner, T.M., Montero, X., Fäshing, D., Galetz, M.C.: Cr diffusion coatings on a ferritic-martensitic steel for corrosion protection in KCl-rich biomass co-firing environments. Corros. Sci. **164**, 108343 (2020). https://doi.org/10.1016/j.corsci.2019.108343
26. Sadeghimeresht, E., Reddy, L., Hussain, T., Huhtakangas, M., Markocsan, N., Joshi, S.: Influence of KCl and HCl on high temperature corrosion of HVAF-sprayed NiCrAlY and NiCrMo coatings. Mater. Des. **148**, 17–29 (2018). https://doi.org/10.1016/j.matdes.2018.03.048
27. Sadeghimeresht, I., Reddy, L., Hussain, T., Markocsan, N., Joshi, S.: Chlorine-induced high temperature corrosion of HVAF-sprayed Ni-based alumina and chromia forming coatings. Corros. Sci. **132**, 170–184 (2018). https://doi.org/10.1016/j.corsci.2017.12.033
28. Jafari, R., Sadeghimeresht, E., Farahani, T.S., Huhtakangas, M., Markocsan, N., Joshi, S.: KCl-induced high-temperature corrosion behaviour of HVAF-sprayed Ni-based coatings in ambient air. J. Therm. Spray Technol. **27**, 500–511 (2018). https://doi.org/10.1007/s11666-017-0684-9
29. Fantozzi, D., Kiilakoski, J., Koivuluoto, H., Vuoristo, P., Uusitalo, M., Bolelli, G., Testa, V., Lusvarghi, L.: High Temperature Corrosion Properties of Thermally Sprayed Ceramic Oxide Coatings. In: Proceedings of International Thermal Spray Conference (2018), Orlando, USA, 501–507 (2018). https://doi.org/10.31399/asm.cp.itsc2018p0501
30. Luo, X., Ning, Z., Zhang, L., Lin, R., He, H., Yang, J., Yang, Y., Liao, J., Liu, N.: Influence of Al_2O_3 overlay on corrosion resistance of plasma sprayed yttria-stabilized zirconia coating in NaCl-KCl molten salt. Surf. Coat. Technol. **361**, 432–437 (2019). https://doi.org/10.1016/j.surfcoat.2019.01.054
31. Ishitsuka, T., Nose, K.: Stability of protective oxide films in waste incineration environment—solubility measurement of oxides in molten chlorides. Corros. Sci. **44**(2), 247–263 (2002). https://doi.org/10.1016/S0010-938X(01)00059-2
32. Lehmusto, J., Skrifvars, B.-J., Yrjas, P., Hupa, M.: Comparison of potassium chloride and potassium carbonate with respect to their tendency to cause high temperature corrosion of stainless 304L steel. Fuel Process. Technol. **105**, 98–105 (2013). https://doi.org/10.1016/j.fuproc.2011.12.016

Publisher's note Springer Nature remains neutral with regard to jurisdictional claims in published maps and institutional affiliations.